Desalination and Water Treatment
www.deswater.com
doi: 10.1080/19443994.2013.768385

51 (2013) 5113–5120
July

Taylor & Francis
Taylor & Francis Group

Performance improvement of countercurrent-flow direct contact membrane distillation in seawater desalination systems

Chii-Dong Ho*, Tz-Jin Yang, Yu-Chuan Chuang

Energy and Opto-Electronic Materials Research Center, Department of Chemical and Materials Engineering, Tamkang University, Tamsui, New Taipei 251, Taiwan
Tel. +886 26215656×2724; Fax: +886 2 26209887; email: cdho@mail.tku.edu.tw

Received 3 June 2012; Accepted 9 September 2012

ABSTRACT

The modeling equations for the temperature distribution and pure water productivity in a parallel-plate direct contact membrane distillation module under countercurrent-flow were derived theoretically with the use of the mass balance on each subchannel. The analytical solution is obtained by using the separated variables method with an orthogonal expansion technique extended in power series. The pure water productivity, average Nusselt number, and temperature distributions of both hot and cold feed streams are represented graphically with the feed velocity and the inlet saline temperature as parameters. The improvements of device performance were achieved under the countercurrent-flow operation. The influences of operation and design parameters on the pure water productivity are also discussed.

Keywords: Conjugated Graetz problems; Countercurrent; Nusselt number; Direct contact membrane distillation; Pure water productivity

1. Introduction

Membrane-based separation processes have been widely used in concentrating or purifying systems, as referred to the membrane contactors, such as desalination processes [1,2] and other applications such as temperature sensible separation [3], waste water treatment [4], juice concentration [5], and other innovative applications [6]. Membrane distillation (MD) modules are more economically attractive in reducing additional energy requirements than conventional distillation processes. It is easy to scale-up the operating device in implementing different membrane processes under lower operating pressure and temperature can be easily incorporated with renewable energy equipment such as solar collectors [7] and solar distillers [8]. The direct contact membrane distillation (DCMD) device in this study is an MD operation for which liquids directly contact both membrane surfaces and provide a phase-change process that only permits vapor transport across a hydrophobic porous membrane to be collected as pure water.

The MD process analysis in countercurrent operations was developed making simultaneous mass and energy balances between both cold and hot feed streams to obtain a two-dimensional microscopic modeling in determining the temperature profiles

*Corresponding author.

7th Aseanian Membrane Society Conference (AMS7), 4–7 July 2012, Busan, Korea

with position in the flow direction and developing the transmembrane flux mechanism as well. The resultant partial differential equations belong to multi-phase or multistream systems with coupling through conjugated conduction-convection conditions on the boundaries, as referred to conjugated Graetz problems [9,10]. The analytical solutions for such conjugated Graetz problems were essentially performed using orthogonal expansion techniques [11–13] in terms of eigenfunctions expansion. Once the temperature distributions and the amount of vapor flux across the membrane are calculated, analytical simplified expressions of Nusselt number and pure water productivity are thus obtained.

This study investigates the heat and mass transfer of the countercurrent flow in DCMD processes to achieve the analytical solution using the separated variables method with an orthogonal expansion technique extended in power series to calculate the Nusselt number and temperature distributions analytically.

1.1. Mathematical statements

Fig. 1 shows a MD module with inserting a hydrophobic microporous membrane of thickness δ_m into a parallel conduit of width B and length L with thickness W_a and W_b for hot and cold feed streams, respectively, to conduct a countercurrent double-flow operation. Hot and cold streams enter subchannels a and b, respectively, as the pure water production process proceeds. The distillate flux of pure water is collected by an overflow tank into a beaker, measured using a timer and weighted on an electronic balance. The mathematical formulations for the transport phenomena of such devices belong to the category of conjugated Graetz problems and can be solved analytically using the eigenfunction expansion technique with the orthogonality conditions [13,14]. The assumptions are: (a) steady-state operation; (b) constant physical properties calculated at some specified temperature; (c) only velocity components in the z-axis direction will be present; (d) no internal generation of energy; (e) fully developed velocity profile. The velocity distributions and equations of energy in dimensionless form for fully developed laminar flow of fluids with negligible longitudinal conduction in a flat-plate geometry may be obtained as [15]

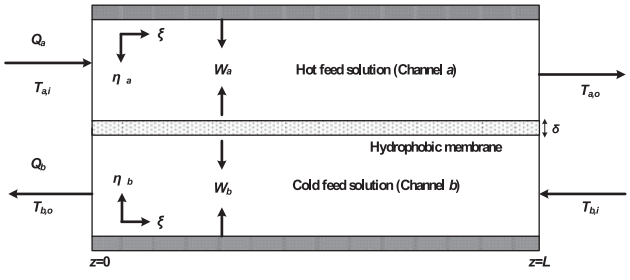

Fig. 1. Schematic diagram of countercurrent MD system in rectangular coordinate.

$$\left[\frac{v_a W_a^2}{L\alpha_a}\right]\frac{\partial\psi_a(\eta_a,\xi)}{\partial\xi}=\frac{\partial^2\psi_a(\eta_a,\xi)}{\partial\eta_a^2} \tag{1}$$

$$\left[\frac{v_b W_b^2}{L\alpha_b}\right]\frac{\partial\psi_b(\eta_b,\xi)}{\partial\xi}=\frac{\partial^2\psi_b(\eta_b,\xi)}{\partial\eta_b^2} \tag{2}$$

$$v_a(\eta_a)=\overline{v_a}\left[6\eta_a-6\eta_a^2\right],\ 0\leqslant\eta_a\leqslant 1 \tag{3}$$

$$v_b(\eta_b)=\overline{v_b}\left[6\eta_b-6\eta_b^2\right],\ 0\leqslant\eta_b\leqslant 1 \tag{4}$$

where

$$\overline{v_a}=\overline{v_b}=Q,\eta_a=\frac{x_a}{W_a},\eta_b=\frac{x_b}{W_b},\xi=\frac{z}{L},\psi_a=\frac{T_a}{T_{a,in}},\psi_b=\frac{T_b}{T_{a,in}},\mathrm{Gz}_a=\frac{\overline{v_a}W_a^2}{4L\alpha_a},\mathrm{Gz}_b=-\frac{\overline{v_b}W_b^2}{4L\alpha_b} \tag{5}$$

The boundary conditions for solving Eqs. (1) and (2) based on the heat transfer mechanism [16] are

$$\psi_a(\eta_a,0)=\psi_{a,in} \tag{6}$$

$$\psi_b(\eta_b,1)=\psi_{b,in} \tag{7}$$

$$\frac{\partial\psi_a(0,\xi)}{\partial\eta_a}=0 \tag{8}$$

$$\frac{\partial\psi_b(0,\xi)}{\partial\eta_b}=0 \tag{9}$$

$$-k_{fa}\frac{\partial\psi_a(1,\xi)}{\partial\eta_a}=W_a\left[N''\lambda+\frac{k_m}{\delta_m}(\psi_a(1,\xi)-\psi_b(1,\xi))\right] \tag{10}$$

$$\frac{\partial\psi_a(1,\xi)}{\partial\eta_a}=-\frac{k_{fb}W_a}{k_{fa}W_b}\frac{\partial\psi_b(1,\xi)}{\partial\eta_b} \tag{11}$$

Eq. (10) expresses that the amount of heat conduction transferred across the membrane is equal to the latent heat accompanying vapor flux, while Eq. (11) indicates the same amount of heat flux occurs at the

mutual boundary. The general expression of mass flux in Eq. (10) was written as

$$N'' = c_{\mathrm{m}}\Delta P^{\mathrm{sat}} = c_{\mathrm{m}}(P_1^{\mathrm{sat}} - P_2^{\mathrm{sat}}) \tag{12}$$

and P_1^{sat}, P_2^{sat} are the saturated pressure of water on the hot and cold feed membrane surfaces, respectively. The membrane coefficient in determining the mass flux across the hydrophobic porous membrane is proposed by Chen et al. [15] and presented by a semi-empirical equation to describe the water vapor flux through a de-aerated microporous membrane, and this is

$$\begin{aligned} c_m &= c_K + c_p \\ &= 1.064\alpha(T)\frac{\varepsilon r}{\tau\delta_m}\left(\frac{M}{RT_m}\right)^{1/2} + 0.125\beta(T)\frac{\varepsilon r^2\ MP_m}{\tau\delta_m\eta_v RT_m} \end{aligned} \tag{13}$$

where $\alpha(T)$ and $\beta(T)$ are the Knudsen diffusion model and Poiseuille flow model contributions, respectively. The vapor pressure within the membrane is not directly measurable and can be expressed in terms of temperatures as $T_1 - T_2 < 15$ [17], that is,

$$N'' = c_m\frac{P_m\lambda M}{RT_m^2}(T_1 - T_2) \tag{14}$$

where $P_m = (P_1^{\mathrm{sat}} + P_2^{\mathrm{sat}})/2$ and $T_m = (T_1 + T_2)/2$ are the mean saturated pressure and mean temperature in membrane, respectively. Substitution of Eq. (14) into Eq. (11) gives

$$\begin{aligned} \frac{\partial\psi_a(1,\xi)}{\partial\eta_a} &= -\frac{\left(c_m \times \frac{P_m\lambda^2 M}{RT_m^2} + \frac{k_m}{\delta_m}\right)}{k_{fa}} W_a[\psi_a(1,\xi) - \psi_b(1,\xi)] \\ &= -H_1 W_a[\psi_a(1,\xi) - \psi_b(1,\xi)] \end{aligned} \tag{15}$$

The analytical solution to this conjugated problem may be obtained using an orthogonal expansion technique in power series. The variable separation leads to the following form:

$$\psi_a(\eta_a,\xi) = \sum_{m=0}^{\infty} S_{a,m}F_{a,m}(\eta_a)G_m(\xi) \tag{16}$$

$$\psi_b(\eta_b,\xi) = \sum_{m=0}^{\infty} S_{b,m}F_{b,m}(\eta_b)G_m(\xi) \tag{17}$$

where $S_{a,m}$ and $S_{b,m}$ are the expansion coefficient associated with eigenfunction $F_{a,m}$ and $F_{b,m}$, respectively, in terms of the eigenvalue λ_m, and G_m is a function of ξ and will be damped out exponentially. Without loss of generality, we may assume the eigenfunctions $F_{a,m}(\eta)$ and $F_{b,m}(\eta)$ to be polynomials, then expressed in the following forms [18]:

$$F_{a,m}(\eta_a) = \sum_{n=0}^{\infty} d_{mn}\eta_a^n, d_{m1} = 0, d_{m0} = 1 \text{ (selected)} \tag{18}$$

$$F_{b,m}(\eta_b) = \sum_{n=0}^{\infty} e_{mn}\eta_b^n, e_{m1} = 0, e_{m0} = 1 \text{ (selected)} \tag{19}$$

All the coefficients d_{mn} and e_{mn} may be in terms of eigenvalue λ_m as

$$\begin{aligned} d_{m2} &= 0 \\ d_{m3} &= 4\mathrm{Gz}_a\lambda_m \\ &\vdots \\ d_{mn} &= \frac{24\mathrm{Gz}_a\lambda_m}{n(n-1)}\left[d_{m(n-3)} - d_{m(n-4)}\right]\ n = 4,5,6\cdots \end{aligned} \tag{20}$$

and

$$\begin{aligned} e_{m2} &= 0 \\ e_{m3} &= -4\mathrm{Gz}_b\lambda_m \\ &\vdots \\ e_{mn} &= -\frac{24\mathrm{Gz}_b\lambda_m}{n(n-1)}\left[e_{m(n-3)} - e_{m(n-4)}\right],\ n = 4,5,6\ldots \end{aligned} \tag{21}$$

The orthogonality conditions in this countercurrent flow MD system for $\lambda_m \neq \lambda_n$ can be expressed to calculate the expansion coefficients $S_{a,m}$ and $S_{b,m}$ as follows:

$$\begin{aligned} &k_{fa}W_b\int_0^1\left[\frac{W_a^2 v_a(\eta_a)}{L\alpha_a}\right]S_{a,m}S_{a,n}F_{a,m}F_{a,n}d\eta_a \\ &\quad + k_{fb}W_a\int_0^1\left[\frac{W_b^2 v_b(\eta_b)}{L\alpha_b}\right]S_{b,m}S_{b,n}F_{b,m}F_{b,n}d\eta_b = 0 \end{aligned} \tag{22}$$

Besides, the relationship between $S_{a,m}$ and $S_{b,m}$ may also be obtained as

$$S_{b,m} = \frac{\left[F'_{a,m}(1) + H_1W_aF_{a,m}(1)\right]}{H_1W_aF_{b,m}(1)}S_{a,m}, \quad m \neq 0 \tag{23}$$

By following the same calculation procedure performed in the previous work [13,14], the coefficients for $S_{a,m}$ and $S_{b,m}$ were calculated as follows:

(i) $m = 0$

$$\begin{aligned} &4\mathrm{Gz}_a\psi_{ai} + \frac{4\mathrm{Gz}_bW_ak_{fb}\psi_{bi}}{W_bk_{fa}} = S_{a,0}\left(4\mathrm{Gz}_a + \frac{4\mathrm{Gz}_bW_ak_{fb}}{W_bk_{fa}}\right) + \sum_{q=1}^{\infty}S_{a,q} \\ &\quad\times\frac{1}{\lambda_q}\left\{e^{\lambda_q}F'_{a,q}(1) - \frac{W_ak_{fb}[F'_{a,q}(1) + H_1W_aF_{a,q}(1)]F'_{b,q}(1)}{W_bk_{fa}\qquad H_1W_aF_{b,q}(1)}\right\} \end{aligned} \tag{24}$$

(ii) $m \neq 0$ and $m = q$

$$\frac{F'_{a,m}(1)\psi_{ai}}{\lambda_m} - \frac{e^{-\lambda_m}\psi_{bi}W_a k_{fb}[F'_{a,m}(1)+H_1W_aF_{a,m}(1)]F'_{b,m}(1)}{\lambda_m W_b k_{fa} \qquad H_1W_aF_{b,m}(1)}$$
$$= \sum_{q=0}^{\infty} S_{a,q}\left\{\left[F_{a,m}(1)\frac{\partial F'_{a,m}}{\partial\lambda_m}(1) - \frac{\partial F_{a,m}}{\partial\lambda_m}(1)F'_{a,m}(1)\right] - \frac{W_a k_{fb}[F'_{a,m}(1)+H_1W_aF_{a,m}(1)]^2}{W_b k_{fa} \qquad (H_1W_a)^2F^2_{b,m}(1)}\left[F_{b,m}(1)\frac{\partial F'_{b,m}}{\partial\lambda_m}(1) - \frac{\partial F_{b,m}}{\partial\lambda_m}(1)F'_{b,m}(1)\right]\right\} \quad (25)$$

(iii) $m \neq 0$ and $m \neq q$

$$\frac{F'_{a,m}(1)\psi_{ai}}{\lambda_m} - \frac{e^{-\lambda_m}\psi_{bi}W_a k_{fb}[F'_{a,m}(1)+H_1W_aF_{a,m}(1)]F'_{b,m}(1)}{\lambda_m W_b k_{fa} \qquad H_1W_aF_{b,m}(1)} = S_{a,0}\times\frac{1}{\lambda_m}\left\{e^{-\lambda_m}F'_{a,m}(1) - \frac{W_a k_{fb}[F'_{a,m}(1)+H_1W_aF_{a,m}(1)]F'_{b,m}(1)}{W_b k_{fa} \qquad H_1W_aF_{b,m}(1)}\right\}$$
$$+\sum_{q=1}^{\infty} S_{a,q}\left\{\frac{e^{\lambda_q-\lambda_m}}{\lambda_m-\lambda_q}[F'_{a,m}(1)F_{a,q}(1) - F_{a,m}(1)F'_{a,q}(1)] - \frac{W_a k_{fb}[F'_{a,m}(1)+H_1W_aF_{a,m}(1)][F'_{a,q}(1)+H_1W_aF_{a,q}(1)]}{W_b k_{fa} \qquad (\lambda_m-\lambda_q)(H_1W_a)^2F_{b,m}(1)F_{b,q}(1)}\right.$$
$$\left.\times[F'_{b,m}(1)F_{b,q}(1) - F_{b,m}(1)F'_{b,q}(1)]\right\} \quad (26)$$

While the expansion coefficients $S_{a,m}$ and $S_{b,m}$ in Eqs. (23) and (24)–(26) are calculated, the average temperature along the flowing direction of both streams were obtained with the aid of Eqs. (16) and (17), and $F_{a,0}(\eta_a) = F_{b,0}(\eta_b) = 1$ with $\lambda_0 = 0$

$$\overline{\psi_a}(\xi) = S_{a,0} + \frac{1}{4\mathrm{Gz}_a}\sum_{m=1}^{\infty}\frac{1}{\lambda_m}S_{a,m}F'_{a,m}(1)e^{\lambda_m\xi} \quad (27)$$

$$\overline{\psi_b}(\xi) = S_{b,0} - \frac{1}{4\mathrm{Gz}_b}\sum_{m=1}^{\infty}\frac{1}{\lambda_m}S_{b,m}F'_{b,m}(1)e^{\lambda_m\xi} \quad (28)$$

2. Average Nusselt number

The local Nusselt number in the hot saline stream is defined by

$$\mathrm{Nu}_\xi = \frac{h_{a\xi}D_{eq,a}}{k_{fa}} = \frac{2\sum_{m=1}^{\infty}S_{a,m}F'_{a,m}(1)e^{\lambda_m\xi}}{\sum_{m=1}^{\infty}S_{a,m}[F_{a,m}(1) - \frac{1}{4\mathrm{Gz}_a\lambda_m}F'_{a,m}(1)]e^{\lambda_m\xi}} \quad (29)$$

where $h_{a\xi}$ is the local heat transfer coefficient for hot saline stream and $D_{eq,a} = 2W_a$ is the equivalent diameter of subchannel a

$$h_{a\xi} = \frac{k_{fa}\ \ \partial\psi_a(1,\xi)/\partial\eta_a}{W_a\psi_a(1,\xi) - \overline{\psi_a}(\xi)} \quad (30)$$

The numerator and denominator in Eq. (30) are obtained differentiating Eq. (16) and with the use of Eq. (27) as follows:

$$\partial\psi_a(1,\xi)/\partial\eta_a = \sum_{m=1}^{\infty}S_{a,m}F'_{a,m}(1)e^{\lambda_m\xi} \quad (31)$$

$$\psi_a(1,\xi) - \overline{\psi_a}(\xi) = \sum_{m=1}^{\infty}S_{a,m}[F_{a,m}(1) - \frac{1}{4\mathrm{Gz}_a\lambda_m}F'_{a,m}(1)]e^{\lambda_m\xi} \quad (32)$$

Substitutions of Eqs. (31) and (32) into Eq. (30) in giving the final expression of the local Nusselt number in Eq. (29). Hence, the average Nusselt number was obtained as

$$\overline{\mathrm{Nu}} = \int_0^1 \mathrm{Nu}_\xi d\xi \quad (33)$$

A numerical example with some equipment parameters and physical properties of some temperature-dependent parameters are assumed to be constant and calculated at the specified temperature and then plugged into the theoretical prediction procedure for simulating real systems. The design parameters, operation parameters and physical properties for both pure water runs and 3.5 wt% NaCl solutions are employed in the present study. $C_{p,a} = 4001\,\mathrm{J/(kg\ K)}$; $C_{p,b} = 4180\,\mathrm{J/(kg\ K)}$; $W_a = W_b = 0.002\,\mathrm{m}$; $L = 0.21\,\mathrm{m}$; $B = 0.29\,\mathrm{m}$; $\delta_m = 130\times10^{-6}\,\mathrm{m}$; $M = 0.018\,\mathrm{kg/mol}$; $Q = 0.0086$, 0.0144, 0.0201 and 0.0259 m/s; $\varepsilon = 0.72$; $T_{a,in} = 30$–$45\,^\circ\mathrm{C}$; $T_{b,in} = 25\,^\circ\mathrm{C}$; $\rho_{\mathrm{NaCl}} = 2170\,\mathrm{kg/m^3}$; $\rho_{b,in} = 998.2\,\mathrm{kg/m^3}$; $\lambda = 2.426\times10^6\,\mathrm{J/kg}$; $k_s = 0.178\,\mathrm{W/(m\,K)}$; $c_m = 5.7\times10^{-7}$ kg/(m^2*Pas*); and $R = 8.314\,\mathrm{J/(mol\ K)}$. Moreover, the correlation equations for some physical properties are

obtained from the experimental data by Ozbek and Phillips [19] as follows:

$$k_g = 0.0144 - 2.16 \times 10^{-5}(T_m + 273.15) + 1.32 \times 10^{-7}(T_m + 273.15)^2 \quad (34)$$

$$k_{fi}(T_{i,in}, m_i) = -0.46 + 5.8 \times 10^{-3}(T_{i,in} + 273.15) - 7.18 \times 10^{-6}(T_{i,in} + 273.15)^2 - 7.3 \times 10^{-3} m_i + 4.1 \times 10^{-4} m_i^2 \; for \; (20 \leqslant T_{i,in} \leqslant 100, 0 \leqslant m_i \leqslant 5) \quad (35)$$

$$\rho_a(T_{a,in}) = \frac{100}{3.5/\rho_{\mathrm{NaCl}} + 96.5/\rho_w} \quad (36)$$

$$\rho_w = 819 + 1.49(T_{in} + 273.15) - 3 \times 10^{-3}(T_{in} + 273.15)^2 \quad (37)$$

$$k_m = \varepsilon k_g + (1 - \varepsilon) k_s \quad (38)$$

3. Results and discussions

Five eigenvalues and the associated expansion coefficients were calculated. Some results for $T_{a,in} = 40$°C, $Q = 0.0259$ m/s as well as the dimensionless outlet temperature and pure water flux are shown in Table 1. The power-series expressions for temperature distributions converge very rapidly and only four eigenvalues as well as their corresponding eigenfunctions are necessary to be considered during the calculation procedure, as suggested from Table 1. The dimensionless temperature distributions in both subchannels for a countercurrent flow device were worked out by analytically solving the governing equations and corresponding boundary conditions as the similar calculation procedure in the previous works [13,14]. The associated eigenfunctions ($F_{a,m}$ and $F_{b,m}$, $m = 0, 1, 2, 3$) can also be found in Eqs. (18) and (19) after the eigenvalues ($\lambda_m, m = 0, 1, 2, 3$) were calculated. Therefore, the temperature distributions of the hot or cold feed stream $\psi_a(\eta_a, \xi)$ or $\psi_b(\eta_b, \xi)$ in the MD are readily gained in Eqs. (16) and (17) with the use of the expansion coefficients ($S_{a,m}$ and $S_{b,m}$, $m = 0, 1, 2, 3$), as shown in Eqs. (23)–(26).

Fig. 2 presents the graphical representations of the theoretical predictions of pure water flux utilizing saline water versus as hot feed streams. The pure water flux increases with increasing feed velocity and inlet hot stream temperature under a given cold feed stream temperature in DCMD systems, as inferred from Fig. 2. The pure water flux increment increases with increasing fluid velocity owing to strengthening the convective heat-transfer coefficient. Restated, the influence of increasing the feed velocity is to reduce both the velocity boundary and the thermal boundary layers, say the disadvantage effect of temperature polarization, resulting in a larger temperature driving force, and hence the transmembrane pressure difference, across the membrane surfaces, as shown in Fig. 2. It was also found that pure water productivity in the countercurrent-flow device was higher than that in the concurrent-flow device. The temperature distributions of both cold and hot feed streams are presented in Fig. 3, while the membrane surface temperatures and wall temperature distributions along the flowing direction are shown in Fig. 4. The temperature gradient between both cold and hot feed streams increases with increasing the feed velocity, and thus, a higher pure water flux was obtained, as observed from Figs. 3 and 4. Besides, the average temperature distributions calculated by Eqs. (27) and (28)

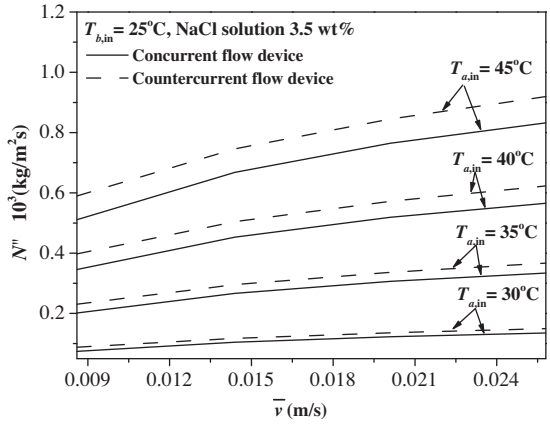

Fig. 2. Pure water flux for saline water versus as the feed velocity of hot stream for both flow patterns.

Table 1
The dimensionless outlet temperature of the hot feed stream for the eigenvalue number and expansion coefficients with analytical solution of pure water flux in countercurrent flow device. $T_{a,in} = 40$°C, $Q = 0.0259$ m/s

m	λ_0	λ_1	λ_2	λ_3	λ_4	$S_{a,0}$	$S_{a,1}$	$S_{a,2}$	$S_{a,3}$	$S_{a,4}$	$\overline{\psi_{a,o}}$	N'' (kg/m² s)
3	0	−0.008	−5.265	–	–	−10.81	11.42	−0.011	–	–	0.9056	5.89×10^{-4}
4	0	−0.008	−5.265	4.990	–	−8.838	9.868	−0.055	-5.87×10^{-6}	–	0.9107	6.23×10^{-4}
5	0	−0.008	−5.265	4.990	−17.16	−8.993	10.024	−0.223	-6.20×10^{-6}	−0.332	0.9109	6.24×10^{-4}

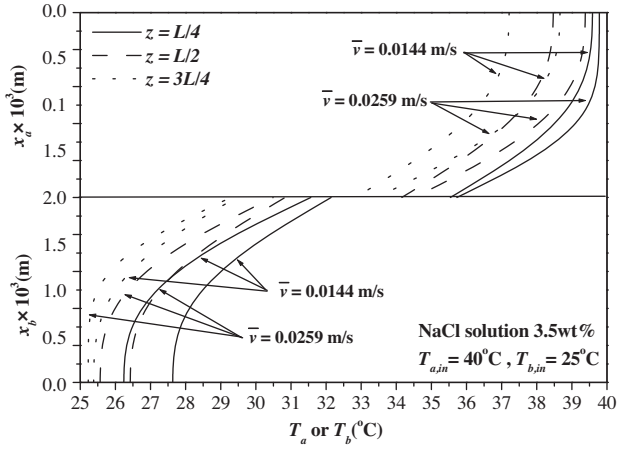

Fig. 3. Temperature distribution profiles in transversal coordinate along flowing direction with $T_{a,in} = 40$℃ and $T_{b,in} = 25$℃.

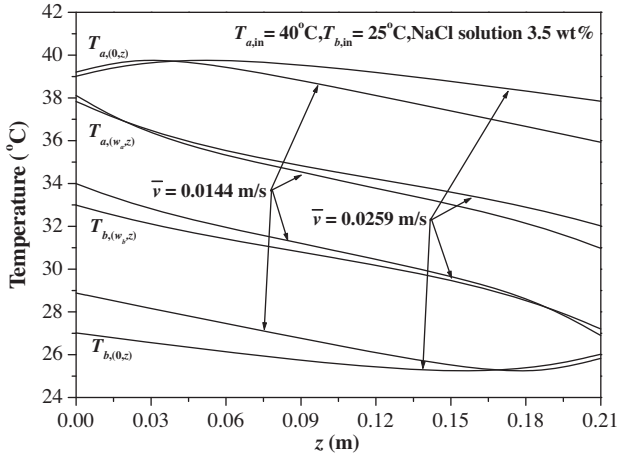

Fig. 4. The wall and membrane surfaces temperature distributions along flowing direction with $T_{a,in} = 40$℃ and $T_{b,in} = 25$℃.

taper along the flow direction in the whole MD module, as indicated from Fig. 5.

The Nusselt number defined by the ratio of convective to conductive heat transfer across the boundary was developed to express the heat transfer efficiency in MD process, and thus, the heat transfer phenomena in longitudinal flowing direction was characterized by the local Nusselt number while the average Nusselt number, was presented for the overall heat transfer efficiency. Fig. 6 shows the theoretical local Nusselt number along the flowing direction with Graetz number in a hot feed stream Gz_a as a parameter. The local Nusselt number has significant enhancement along the hot stream flow direction and increases with increasing Graetz numbers in the hot feed stream as well. Fig. 7 shows the theoretical results of the average Nusselt

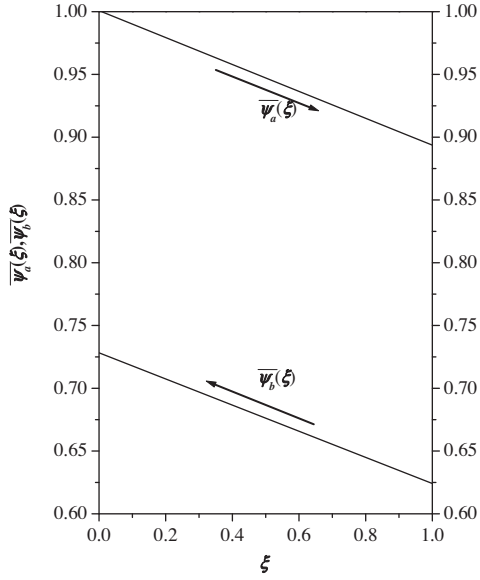

Fig. 5. The dimensionless average temperature distributions in whole MD module with $T_{a,in} = 40$℃, $T_{b,in} = 25$℃ and $\overline{v} = 0.0259$.

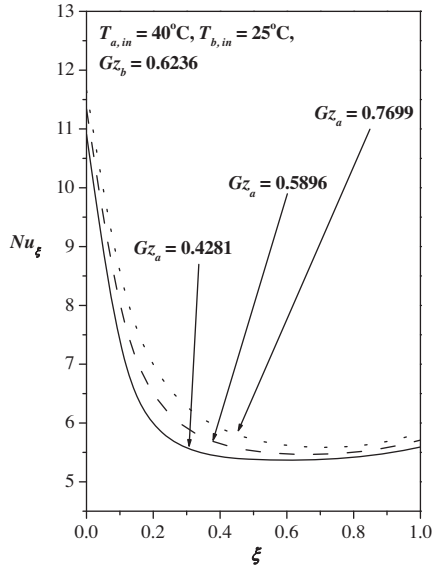

Fig. 6. The local Nusselt number profile in different hot feed stream Gz_a with $T_{a,in} = 40$℃, $T_{b,in} = 25$℃ and $Gz_b = 0.6236$.

number $\overline{Nu}$ of the hot feed stream versus Graetz number variations (Gz_a) in the hot stream under both concurrent- and countercurrent-flow operations. The larger the Graetz number is operated, the larger $\overline{Nu}$ is obtained, regardless of the concurrent- and countercurrent-flow devices, as demonstrated in Fig. 7. Moreover, the average Nusselt number in the countercurrent-flow device is larger than that in the concurrent-flow device, as shown in Fig. 7.

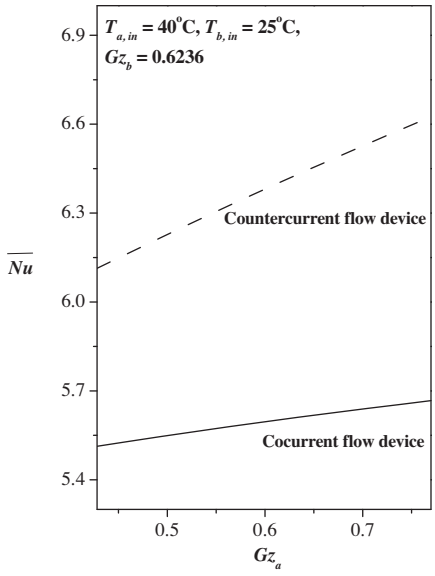

Fig. 7. Comparison of the average Nusselt number with different flow-type devices with $T_{a,in} = 40$°C, $T_{b,in} = 25$°C and $Gz_b = 0.6236$.

4. Conclusions

Heat and mass transfer phenomena of the laminar countercurrent-flow flat-plate membrane distillation modules were analytically investigated in this study. The two-dimensional heat-transfer mathematical formulation with water vapor flux across the membrane was developed theoretically and solved analytically using the orthogonal technique with eigenfunction expanding in terms of a power series. A good approximation was obtained using four eigenvalues in the calculation procedure, as shown in Table 1. The dimensionless temperature profiles in both subchannels, pure water flux, and Nusselt number were calculated and represented graphically. The advantage and value of the theoretical model in this study lie in the fact that they can calculate the Nusselt number and pure water flux directly without experimental runs or semi-experimental equations and yield the dimensionless temperature profile in the entire MD modules under the countercurrent-flow operation. There are many operation and design parameters such as the feed velocity and inlet hot stream temperature that may affect the device performance in the MD modules. It is also found in Figs. 2 and 7, the pure water flux and average Nusselt number increase with increasing feed velocity and Graetz number Gz_a, respectively. Furthermore, the pure water flux and average Nusselt number in the countercurrent-flow device is larger than those in the concurrent-flow device. One can also expect that the present mathematical treatment can be applied to other DCMD modules.

Acknowledgment

The authors thank the National Science Council of the republic of China and Tamkang University for their financial support.

Symbols

B	—	width of the channel, m
C_p	—	heat capacity of feed solution, J/kg K
c_k	—	membrane coefficient based on the Knudsen diffusion model, kg/(m^2 Pa s)
c_m	—	membrane coefficient, kg/(m^{2}Pa s)
c_p	—	membrane coefficient based on the Poiseuille flow model, kg/(m^2 Pa s)
d_{mn}	—	coefficient in the eigenfunction $F_{a,m}$
$D_{eq,a}$	—	the equivalent diameter of subchannel a
e_{mn}	—	coefficient in the eigenfunction $F_{b,m}$
F_m	—	eigenfunction associated with eigenvalue λ_m
G_m	—	function defined during the use of orthogonal expansion method
Gz	—	Graetz number
H_1	—	definition in Eq. (15)
$h_{a\xi}$	—	local heat transfer coefficient for hot feed stream, J/(s m K)
k_f	—	thermal conductivity of feed stream solution, J/(s m K)
k_g	—	proportion of gas pore thermal conductivity, J/(s m K)
k_s	—	solid membrane thermal conductivity, J/(s m K)
k_m	—	thermal conductivity of the porous membrane, J/(s m K)
L	—	channel length, m
M	—	molecular weight of water, kg/mol
m	—	molality of NaCl in NaCl solution
N'	—	pure water flux, kg/(m^{2}s)
Nu_ξ	—	local Nusselt number
$\overline{Nu}$	—	average Nusselt number
P_1^{sat}	—	saturated pressure of water on hot feed membrane surface, Pa
P_2^{sat}	—	saturated pressure of water on cold feed membrane surface, Pa
P_m	—	mean saturated pressure in membrane, Pa
Q	—	feed velocity, m/s
r	—	membrane pore radius, m
R	—	gas constant, J/mol K
S_m	—	expansion coefficient associated with eigenvalue λ_m
T_1	—	temperature of water on hot feed membrane surface, °C

T_2 — temperature of water on cold feed membrane surface, ℃
T — feed stream temperature, ℃
T_{in} — inlet stream temperature, ℃
T_m — mean temperature in membrane, ℃
v — stream velocity, m/s
$\bar{v}$ — mean stream velocity, m/s
W — height of channel, m
X — transversal coordinate, m
Z — longitudinal coordinate, m

Greek symbols

α — thermal diffusion coefficient, m^2/s
$\alpha(T)$ — the Knudsen diffusion model contribution
$\beta(T)$ — the Poiseuille flow model contribution
δ_m — thickness of the porous membrane, m
ε — membrane porosity
η — dimensionless transversal coordinate, x/W
η_v — gas viscosity, $N\,s/m^2$
λ — latent heat of water, J/kg
λ_m — Eigenvalue
ρ — fluid density of feed solution, kg/m^3
ρ_{NaCl} — density of solid NaCl, kg/m^3
ρ_w — density of pure water, kg/m^3
ξ — dimensionless transversal coordinate, z/L
τ — membrane turtuosity factor
ψ — dimensionless temperature
$\overline{\psi}$ — average dimensionless temperature

Subscript

a — in the hot feed stream channel
b — in the cold feed stream channel
con — in the concurrent flow device
counter — in the countercurrent flow device
in — at inlet

References

[1] K.W. Lawson, D.R. Lloyd, Membrane distillation, J. Membr. Sci. 124 (1997) 1–25.
[2] M. Gryta, M. Tomaszewska, J. Grzechulska and A.W. Morawski, Membrane distillation of NaCl solution containing natural organic matter, J. Membr. Sci. 181 (2001) 279–287.
[3] J.M. Ortiz De Zárate, C. Rincón, J.I. Mengual, Concentration of bovine serum albumin aqueous solutions by membrane distillation, Sep. Sci. Technol. 33 (1998) 283–298.
[4] V. Calabro, E. Drioli, F. Matera, Membrane distillation in the textile wastewater treatment, Desalination 83 (1991) 209–224.
[5] V. Calabro, B.L. Jiao, E. Drioli, Theoretical and experimental study on membrane distillation in the concentration of orange juice, Ind. Eng. Chem. Res. 33 (1994) 1803–1808.
[6] Z. Ding, L. Liu, J. Yu, R. Ma, Z. Yang, Concentrating the extract of traditional Chinese medicine by direct contact membrane distillation, J. Membr. Sci. 310 (2008) 539–549.
[7] J. Koschikowski, M. Wieghaus, M. Rommel, Solar thermal-driven desalination plants based on membrane distillation, Desalination 156 (2003) 295–304.
[8] M.C. de Andrés, J. Doria, M. Khayet, L. Peña, J.I. Mengual, Coupling of membrane distillation module to a multieffect distiller for pure water production, Desalination 115 (1998) 71–81.
[9] R.J. Nunge, W.N. Gill, Analysis of heat or mass transfer in some countercurrent flows, Int. J. Heat Mass Transfer 8 (1965) 873–886.
[10] E. Papoutsakis, D. Ramkrishna, Conjugated Graetz problems. I. General formalism and a class of solid-fluid problems, Chem. Eng. Sci. 36 (1981) 1381–1391.
[11] G.M. Brown, Heat or mass transfer in a fluid in laminar flow in a circular or flat conduit, AIChE J. 6 (1960) 179–183.
[12] S.N. Singh, Heat transfer by laminar flow in a cylindrical tube, Appl. Sci. Res. 7 (1958) 237–240.
[13] R.J. Nunge, W.N. Gill, An analytical study of laminar counterflow double-pipe heat exchangers, AIChE J. 12 (1966) 279–289.
[14] W.P. Wang, S.T. Lin, C.D. Ho, An analytical study of laminar co-current flow gas absorption through a parallel-plate gas–liquid membrane contactor, J. Membr. Sci. 278 (2006) 181–189.
[15] T.C. Chen, C.D. Ho, H.M. Yeh, Theoretical modeling and experimental analysis of direct contact membrane distillation, J. Membr. Sci. 330 (2009) 279–287.
[16] R.W. Schofield, A.G. Fane, C.J.D. Fell, Heat and mass transfer in membrane distillation, J. Membr. Sci. 33 (1987) 299–313.
[17] J.S. Chiou, K.T. Cheng, S.T. Hsu, Seawater desalination by direct contact membrane distillation, Desalination 143 (2002) 279–287.
[18] C.D. Ho, H.M. Yeh, W.S. Sheu, An analytical study of heat and mass transfer through a parallel-plate channel with recycle, Int. J. Heat Mass Transfer 41 (1998) 2589–2599.
[19] H. Ozbek, S.L. Phillips, Thermal conductivity of aqueous sodium chloride solutions from 20 to 330.degree C, J. Chem. Eng. Data 25 (1980) 263–267.